

# Masking versus removing point sources in CMB data: the source corrected WMAP power spectrum from new extended catalogue

Sandro Scodeller

*Institute of Theoretical Astrophysics, University of Oslo, P.O. Box 1029 Blindern, N-0315 Oslo, Norway*

`sandro.scodeller@astro.uio.no`

Frode K. Hansen

*Institute of Theoretical Astrophysics, University of Oslo, P.O. Box 1029 Blindern, N-0315 Oslo, Norway;*

*Centre of Mathematics for Applications, University of Oslo, P.O. Box 1053 Blindern, N-0316 Oslo*

`frodekh@astro.uio.no`

## ABSTRACT

In Scodeller et al. (2012) a new and extended point source catalogue obtained from the WMAP 7 year data was presented. It includes most of the sources included in the standard WMAP 7 year point source catalogues as well as a large number of new detections. Here we study the effects on the estimated power spectra when taking the newly detected point sources into consideration. We create point source masks for all the 2102 sources that we detected as well as a smaller one for the 665 sources detected in the Q, V and W bands. We also create WMAP7 maps with point sources subtracted in order to compare with the spectra obtained with source masks. The extended point source masks and point source cleaned WMAP7 maps are made publicly available. Using the proper residual correction, we find that the power spectra obtained from the point source cleaned map without any source mask is fully consistent with the spectra obtained from the masked map. We further find that the spectra obtained masking all 2102 sources is consistent with the results obtained using the WMAP 7 year point source mask. We also verify that the removal of point sources does not introduce any skewness.

*Subject headings:* (cosmology:) cosmic microwave background — cosmology: observations — methods: data analysis — methods: statistical

## 1. Introduction

The study of the Cosmic Microwave Background (CMB) is a fundamental tool for understanding the universe we live in. A very important link from the study of the CMB to parameters describing our universe is the power spectrum  $C_\ell$  of the anisotropies in the CMB (see for instance Larson et al. (2011)). It is hence very important to accurately measure the spectrum  $C_\ell$ , which is obtained via measuring the temperature of the sky, which in turn has contaminating foregrounds. The main contaminants on larger scales are extended foregrounds (diffuse galactic emissions) while on small scales, extra-galactic point sources are the main contaminants (see for instance Toffolatti et al. (1998), De Zotti et al. (1999), Hobson et al. (1999), De Zotti et al. (2005)). The most accurate (meaning high resolution and high signal to noise ratio) publicly available measurements of the CMB anisotropies we have up to today is the Wilkinson Microwave Anisotropy Probe (WMAP) (Bennett et al. 2003). Clearly, measuring the CMB and its anisotropies accurately also implies correcting accurately for the contaminants. In Scodeller et al. (2012), we presented a new way to disentangle the point source signal from the CMB and other foregrounds obtaining a new and extended catalogue of extragalactic sources. The novelty of our approach was the use of needlet transforms (see Marinucci et al. (2008) or Scodeller et al. (2011) and references therein) and internal templates (Hansen et al. (2006)) to enhance the signal to noise ratio of the point source signal.

The point sources contribute to the spectrum mainly at large multipoles  $\ell$  and correcting the power spectrum from the bias which they introduce is crucial for accurately estimating the cosmological parameters. This can be done in two ways: the standard approach is to mask the observed map with a point source mask and then compute the spectrum (see (Larson et al. (2011))). Another approach is to remove the best model estimates of the point sources in the map and then compute the power spectrum, which to our knowledge has been considered in only a very few papers (see Tegmark & de Oliveira-Costa (1998) or Bajkova (2005)). The advantage of the standard approach is that it has no dependence on whether the source is modelled correctly, but each source is masked with a rather large disc depending on the beam of the experiment and some data is lost. Another disadvantage with this approach is that analysis methods applying filters (for instance wavelets) to the map may contaminate an even larger part of the filtered map in the area of the point source holes (see for instance Scodeller et al. (2011)). The alternative approach depends on modelling the source correctly, but less data is masked and filtered maps will not be contaminated by point source holes. In this paper we use both approaches in order to compare them. Even if we increased substantially the number of detected point sources, there are still unresolved point sources which contribute to estimate of the spectrum  $C_\ell$ . We use the approach first presented in Hinshaw et al. (2003) by the WMAP-team to correct for it.

The scope of this paper is threefold:

1. To compare the effect of masking point sources versus removing best fit source models when estimating the CMB power spectrum. We do this by running a large number of simulations with point sources and compare the mean of the estimated spectra using each of the two procedures. Since the WMAP team used only the V and W channels to estimate the power spectrum and to save CPU time, we simulate only the V and W channels.
2. To compare the power spectrum in the WMAP 7-year data using the two different approaches above as well as to see the effect of masking/removing all the additional point sources detected in Scodeller et al. (2012) on the power spectrum
3. To compare the masking and removing approach on the skewness of needlet coefficients.

The outline of the paper is as follows: in section 2 we look at the simulations in general: in subsection 2.1 we show how realistic simulations were obtained, then in subsection 2.2 we present the method used for simulations to estimate the CMB power spectrum  $C_\ell$  and in subsection 2.3 the results of the simulations. Then in section 3 we present the results (and the slight changes to the method) of the WMAP 7 year data. In section 4 we present the results of the skewness analysis. Finally, in section 5 we present our conclusions.

## 2. Simulations

### 2.1. Creating the simulations

To fulfill goals 1 and 3 above, we need to generate an ensemble of realistic simulations of CMB, noise and point sources for the V and W channels. To generate the point source simulations we draw the fluxes from a flux distribution in the V-channel and transform to other channels drawing from a spectral index distribution. For the V-channel, we sample fluxes  $S$  from the distribution for the differential number counts  $\frac{dN}{dS}$  found in (Scodeller et al. 2012),

$$\frac{dN}{dS} \propto S^{-2.14} \quad \forall S > S_{\min},$$

Following Herranz et al. (2006) we chose to sample from  $S_{\min} = 0.08$  Jy, well below the detection limit, till  $6\langle\sigma_V\rangle$ , where  $\langle\sigma_V\rangle \approx 0.222$  Jy is the mean of the error on the estimated fluxes in the V channel. Above  $6\langle\sigma_V\rangle$  we use the actual amplitudes estimated in the WMAP 7 year data. We normalize the distribution function  $dN/dS = nS^{-2.14}$  (giving the number of

sources per Jy per steradian), where  $n$  is a normalization constant, using that in real data we detected 103 sources with fluxes above  $\geq 6\langle\sigma_V\rangle$  (Scodeller et al. 2012),

$$n \int_{6 \times 0.222 J_y}^{\infty} S^{-2.14} dS = 103 / (4\pi f_{\text{sky}}).$$

The total number  $N$  of sources above  $S_{\min}$  for the full sky is then determined by integrating

$$N = n \int_{0.08 J_y}^{\infty} S^{-2.14} dS \times 4\pi = 3082$$

Eventually this gives 2955 simulated fluxes being  $< 6\langle\sigma_V\rangle$ . We then use the actual fluxes of the point sources being  $> 6\sigma_V$  in the V channel and the fluxes estimated in the V-channel of the sources which are  $> 6\sigma_W$  in channel W but  $< 6\sigma_V$  in the V-channel (which add up to 113 sources). We thus obtain a set of 3068 realistic values of fluxes of point sources at frequency V of which 2955 are drawn from the distribution of the differential number counts and 113 are fluxes of strong sources from real data.

In order to obtain realistic values of fluxes in the W-channel, we scale the fluxes  $< 6\langle\sigma_V\rangle$  in the V-channel with a spectral index distribution having mean -0.28 and a dispersion of 0.65. The mean value is chosen half way from the mean spectral index obtained by Lanz et al. (2011) (namely -0.5) and the WMAP-team Nolte et al. (2009) (namely -0.09), while for the dispersion we took the bigger one of the two, i.e. from Lanz et al. (2011).

We therefore sample 2955 values of spectral indices from a gaussian distribution with mean -0.28 and dispersion 0.65 and rescale the simulated fluxes for the V-channel with these spectral indices to simulated fluxes in the W-channel. Similarly to the approach in the V-channel we use the 113 actual fluxes from real data which are bigger then  $> 6\langle\sigma\rangle$  in one of the two channels.

Except for the 113 strong sources, for which we use amplitude and position estimated from real data, the position of the remaining sources are simulated randomly across the full sky. Since in (Scodeller et al. 2012) we identify two point source as the same if their separation is less than  $0.4^\circ$ , we simulate all those sources which are stronger than the smallest detected flux in V-band WMAP data at least  $0.4^\circ$  from each other (but there is no such condition with respect to weaker sources).

In order to get a good estimate on the error of estimated power spectra we create 10000 realisations, for both the V and W channel, of CMB fluctuations (based on the WMAP best-fit  $C_\ell$ ), noise and then add the (same) pure point source map obtained as explained above.

## 2.2. Influence of mask and point source removal on $C_\ell$ : Method

The basic idea is to estimate and compare the power spectra  $C_\ell$  obtained by either removing or masking detected sources. We will estimate the two autospectra VV and WW, the cross-spectrum VW as well as the optimal noise-weighted co-added combination of the autospectra. Our procedure will be applied to the full ensemble of simulated maps as well as to the actual WMAP7 data (with some differences due to the need to save CPU-time for the simulations, this will be detailed later).

Step by step our procedure for the simulations is:

1. We use the detection algorithm presented in (Scodeller et al. 2012) to detect point sources: Sources are counted as detected in the V-band if
  - they are found at  $> 5\sigma$  directly in V.
  - they are found at  $> 5\sigma$  in W: In this case we search in V in a disc of radius  $0.12^\circ$  around the position in W and if a source at  $> 3\sigma$  is found, it is counted as detected in V. This is different from the approach used in Scodeller et al. (2012) where we tested for  $> 5\sigma$  in the internal templates and then searched for  $> 3\sigma$  in the given band (note that the radius of the disc to search was defined from the error bars on the position of the source, this is what we have used to obtain  $0.12^\circ$  in the present case). Since we only simulate the V and W channels, we only have one single internal template available with a small frequency difference making the internal template approach inefficient.

We use the same approach to define detected sources in the W-band.

2. We construct the co-added map defined as the noise weighted sum of the two frequency bands:

$$M_{VW} = w_V M_V + w_W M_W,$$

where  $M_{VW}$  is the combine map,  $M_i$  the map at channel  $i$  and the weights  $w_i$  are given by:

$$w_i = \sum_p 1/\sigma_{pi}^2 / \left( \sum_p 1/\sigma_{pV}^2 + \sum_p 1/\sigma_{pW}^2 \right)$$

with  $\sigma_{pi}$  being the rms in pixel  $p$  of the instrumental noise in channel  $i$  and the sum is over all pixels  $p$ .

3. We multiply the maps  $M_V$ ,  $M_W$  and the co-added map  $M_{VW}$  with the KQ85 galactic mask (we would like to stress *galactic*, no point sources at all are masked in this step).

4. We remove the best fit models of the detected sources in each channel to create the maps  $M_V^R$ ,  $M_W^R$  and  $M_{VW}^R$ .
5. We create a mask which masks the detected sources in each channel with radius of  $0.6^\circ$ <sup>1</sup>. Then we multiply the 3 maps with point sources with the mask obtaining  $M_{VW}^M$ ,  $M_V^M$  and  $M_W^M$ .
6. Estimate the power spectra  $C_\ell$  using the master-algorithm (Hivon et al. 2002) with different channel-combinations obtaining:  $C_\ell^{R,VW}$ ,  $C_\ell^{R,VV}$ ,  $C_\ell^{R,WW}$ ,  $C_\ell^{M,VW}$ ,  $C_\ell^{M,VV}$ ,  $C_\ell^{M,WW}$ . Estimate also the cross-power-spectra  $C_\ell^{R,X}$  and  $C_\ell^{M,X}$ .
7. We now correct for a small bias in the power spectrum introduced by the residuals of the removed sources. We know that at the position of a removed source, there is a residual source with mean zero and standard deviation given by the error bar on the amplitude of the source. Furthermore, this residual sources have a slightly asymmetric form due to the error in the estimated position. We correct for this residual source bias in the power spectrum by taking the mean spectrum of 1000 source subtracted simulated maps where we subtract the pure CMB power spectrum. We use the same approach to check if there are residuals outside the point source holes when masking, but find that the correction in this case is negligible.
8. Correct for the contribution of the unresolved point sources contribution following the method of the WMAP team, first presented in Hinshaw et al. (2003). In order to simplify the procedure without compromising the scope of the simulations, we have made the following changes in the procedure in Hinshaw et al. (2003):
  - we use the band average (not the different DAs per band) spectra
  - we use the only three available spectra (VV, VxW and WW), hence also using auto-spectra
  - in the calculation of the correlation matrix  $\Sigma_{\ell\ell}^{\alpha\beta}$ , the WMAP team uses a multipole dependent sky fraction  $f_{sky}(\ell)$  based on an effective noise power. Here instead, we use a slightly simplified procedure to obtain  $f_{sky}(\ell)$  calibrated from 10000 simulations of CMB+noise. A bit more in detail, we compute the standard deviation of the estimated power spectra  $\Delta\hat{C}_\ell$  of the 10000 simulations (as usual via the master-algorithm). Then we obtain  $f_{sky}(\ell)$  from:

---

<sup>1</sup>NB: in analogy to the WMAP approach, we use the same mask for the V and W channels, hence masking for instance a source in W, which is only detected in V.

$$f_{sky}(\ell) = \sqrt{\frac{2}{2\ell+1}} \frac{C_\ell + N_\ell}{\Delta \hat{C}_\ell}, \quad (1)$$

where  $C_\ell$  is the best-fit power spectrum from WMAP (input in the simulations) and  $N_\ell$  is the noise power, computed with the mask of the galaxy only (if removing) or a galaxy and point source mask taken from a simulation with the average number of detections (if masking)

- we use only uniform pixel weighting (not inverse noise weighting for high multipoles  $\ell$ )
- define the covariance matrix  $\Sigma_{\ell\ell}^{\alpha\beta}$ , where  $\alpha$  and  $\beta$  are channel combinations (VV, VxW or WW)), with  $f_{sky}(\ell)$  and  $N_\ell$  obtained either with a galaxy only mask (when removing) or from a galaxy and point source mask taken from a simulation with the average number of detected point sources.
- The error on the estimated amplitude  $A_{ps}$  is given by the standard deviation of  $A_{ps}$  of the 9000 simulations (only 9000, because we used 1000 simulations for estimating the bias of the residuals).

### 2.3. Simulations: Results

In figures 1 (removed point sources) and 2 (difference between masked and removed) we show the average spectra obtained from the 9000 simulations from the combined map  $M_{VW}$ . The results are very similar for the VV, WW autospectra and VxW cross-spectrum, we only show the co-added V+W results here. In the top plot of the first figure we show the whole  $\ell$ -range before and after the correction of unresolved point source contribution, while in the bottom plot we show the high multipole range (600 to 1000). We also show the size of the bias introduced by the point source residuals (difference between top black curve and grey curve), as one would expect it becomes non-negligible only at high multipoles ( $\ell \gtrsim 700$ ).

We would like to point out that in some of the autospectra a small bias is present at high multipoles, which disappears if we redo the simulations with constant spectral index. The reason for this small bias is that the method for subtracting unresolved point sources (Hinshaw et al. 2003) assumes a constant spectral index and we found that a tiny bias appears in the realistic case with varying spectral index. This bias is present at the same level for both for source removal and source masking.

One of the reasons why we try two approaches (masking and removing) is that if one removes the point sources instead of masking them one uses a bigger part of the sky (and

hence more information) to compute the CMB power spectrum. One would therefore expect that the standard deviation of the power spectra found in the 9000 simulations are smaller when we remove the point sources instead of masking them. This is indeed the case as we show in figure 3, where we see the relative difference between the standard deviation of the masking approach  $\sigma(C_\ell^{M,VW})$  and the removing approach  $\sigma(C_\ell^{R,VW})$  normalized to the (standard) masking approach. The increase in accuracy is expected to become substantial from the multipoles which are close in angular extension to the size of the holes (the point sources are masked with a hole of radius  $0.6^\circ \rightarrow \ell \sim 300$ ) till where the increase in information is counter-balanced by the noise. Note that in some realistic experiments, beam asymmetries may be so large that systematic errors in the point source removal procedure may partially cancel the decrease in error bars due to increased sky fraction.

### 3. WMAP 7 year data

#### 3.1. Method

The method to estimate the power spectra for real data is slightly different to the one for the simulations. The differences are in the followings steps from the description of the method for simulations (see section 2.2) :

1. We use the 665 detected point sources as presented in Scodeller et al. (2012) in the Q, V and W channel. We use both the point sources which were detected at  $5\sigma$  in the channels and those detected at  $5\sigma$  in the templates and at  $3\sigma$  in channels. This is different from the simulations, where, due to the limited number of frequency channels in the simulations, we did not use internal templates but instead looked for  $3\sigma$  in V where there was a  $5\sigma$  in W and vice versa.
4. Remove the detected point sources both from the band averaged Q,V and W channels as well as from the 8 individual differencing assemblies (DAs) Q1 till W4.
5. Like in the preceding step, mask both the band averaged channels and the DAs.
7. To correct for the residual point source bias in the power spectrum, we use the same procedure as for the simulations, but the input sources used in the simulations were all taken from actual values estimated in real data for all channels. We only estimate the power spectra in the V and W bands, so in principle the Q band is not needed. However, to estimate the contribution of unresolved sources in real data, we also need the Q band to get smallest possible error bars (note that we need the Q band only



to obtain the contribution of unresolved sources, it is not used further). This means that we also need to remove sources in the Q band and correct for the residual sources. In order to save CPU time and avoid having to run full simulations for the Q band to obtain the residual source correction, we run simplified simulations which we have verified give consistent values for the unresolved source contributions. This consists in pure source simulations where we subtract random model sources based on the standard deviations of the estimated amplitudes and positions. The only difference with the full approach used for the V and W band is that the correlation between estimated amplitude and the background CMB and noise is missing.

8. In order to better compare the amplitude of the unresolved point source-contribution  $A_{ps}$  to the one obtained by the WMAP-team (Larson et al. (2011)) we compute it using all 28 DA cross combinations (eg. Q1Q2,Q1V2,W3W4, etc.), otherwise we use the same approximations as for the simulations. We assume the same spectral index as the WMAP team, -2.09.

Additionally, we do not only remove or mask as in simulations, but (both when removing and masking) we use different kinds of masks. First of all we use KQ85yr7 mask to check whether we obtain the same value of the unresolved point source contribution amplitude as the WMAP-team, obtaining:  $A_{ps}^{M,KQ85} = 9.18 \pm 1.14 [10^3 \mu K^2]$ . This is in good agreement with the value obtained by the WMAP team:  $9.0 \pm 0.7 [10^3 \mu K^2]$  (Larson et al. (2011)). We point out that the error on  $A_{ps}$  is now calculated the same way as by the WMAP team (see Hinshaw et al. (2003)). The reason that the error on the estimated  $A_{ps}$  we obtain is bigger than the one of the WMAP team is due to a combination of using only a uniform weighting, having a different  $f_{sky}(\ell)$  and having a different noise power entering the covariance matrix  $\Sigma_{\ell\ell}^{\alpha\beta}$  making the estimator slightly non-optimal. These simplifications which lead to slightly larger error bars do not compromise the scope of this paper.

Then we use the following masking schemes:

**Basic mask** We only remove respectively mask the 665 detected point sources from the maps<sup>2</sup> and use the galaxy mask to obtain the amplitude  $A_{ps}$  and the combined spectra  $\rightarrow A_{ps}^R$  and  $C_\ell^{R,\alpha}$  respectively  $A_{ps}^M$  and  $C_\ell^{M,\alpha}$  with  $\alpha$  being a combination of channels or DAs;

---

<sup>2</sup>the 665 point sources are detected ( $5\sigma$  in the channels or  $5\sigma$  in the template and  $3\sigma$  in the channel) in at least Q, V or W band, not forcefully in all 3 channels, when masking we mask all 665 independently of the channel.

**Extended Mask** We check for any remnant wavelet coefficients at  $> 5\sigma$  after removing or masking the point sources and extend the galactic mask with a disc of  $0.6^\circ$  around these pixels

$$\rightarrow A_{ps,ext}^R \text{ and } C_{\ell,ext}^{R,\alpha} \text{ respectively } A_{ps,ext}^M \text{ and } C_{\ell,ext}^{M,\alpha};$$

**Extended mask including KQ85** Include the KQ85 mask (7-year WMAP release) from the WMAP team. When masking: multiplying the extended mask by the KQ85 mask. When removing: only putting to zero the point sources of the KQ85 mask which do not coincide with any of the removed 665 sources.

$$\rightarrow A_{ps,extKQ85}^R \text{ and } C_{\ell,extKQ85}^{R,\alpha} \text{ respectively } A_{ps,extKQ85}^M \text{ and } C_{\ell,extKQ85}^{M,\alpha};$$

**All 1116** Consider all the 1116 point sources which in (Scodeller et al. (2012)) were found to be either at  $5\sigma$  directly in any of the 5 WMAP frequency channels or at  $5\sigma$  in internal templates and at  $3\sigma$  in any of the channels. When removing: remove the above 665 sources and mask the rest.

$$\rightarrow A_{ps,1116}^R \text{ and } C_{\ell,1116}^{R,\alpha} \text{ respectively } A_{ps,1116}^M \text{ and } C_{\ell,1116}^{M,\alpha};$$

**All 1116 include KQ85** Like before include the mask from the WMAP team.

$$\rightarrow A_{ps,1116KQ85}^R \text{ and } C_{\ell,1116KQ85}^{R,\alpha} \text{ respectively } A_{ps,1116KQ85}^M \text{ and } C_{\ell,1116KQ85}^{M,\alpha};$$

**All 2102** Consider all the 2102 different point sources which in (Scodeller et al. (2012)) were detected either at  $5\sigma$  in any of the channels or at  $5\sigma$  in any of the templates (without the need for a  $3\sigma$  in any of the channels). Like for the 1116 approach, when removing, remove the above 665 sources and mask the rest.

$$\rightarrow A_{ps,2102}^R \text{ and } C_{\ell,2102}^{R,\alpha} \text{ respectively } A_{ps,2102}^M \text{ and } C_{\ell,2102}^{M,\alpha};$$

**All 2102 including KQ85** Like before include the mask from the WMAP team.

$$\rightarrow A_{ps,2102KQ85}^R \text{ and } C_{\ell,2102KQ85}^{R,\alpha} \text{ respectively } A_{ps,2102KQ85}^M \text{ and } C_{\ell,2102KQ85}^{M,\alpha};$$

These different masks and the pure point source maps for each DA (which were used to subtract from the temperature maps to obtain clean maps), as well as the residual corrections for the spectra obtained when removing, are available on [http://folk.uio.no/frodekh/PS\\_catalogue/](http://folk.uio.no/frodekh/PS_catalogue/). The only difference between the pure point source correction maps for the same frequency band is the difference in beam between the DAs. In order to use these correction maps with for instance band averaged temperature maps, one can use one of these correction maps for one DA, deconvolve with the beam for the given DA and convolve with the desired beam.

In table 1 we show different values we obtain for the amplitude of the unresolved point source contribution  $A_{ps}$ .

As expected, when removing sources, the error on the estimated amplitude  $A_{ps}$  are slightly smaller than when masking. This is a consequence of having a bigger sky-fraction and hence more information. In Nolita et al. (2009) the WMAP-team says that their estimate of  $A_{ps}$  is independent of the mask used (when calculating it with Q,V and W DAs). While in our case it is very dependent on the mask. This is though no contradiction since they use always the same point-source-mask but change only the galactic cut (they use KQ75, KQ80 and KQ85), while our masks all include the same galactic mask, but with a varying number of point source holes. The masks with many point source holes mask more sources than the WMAP point source mask (in Scodeller et al. (2012) we resolved more point sources than the WMAP team) and hence the number of unresolved sources decreases.

With respect to the power spectra obtained, there is no substantial difference between which mask we use or whether we remove or mask the point sources, as long as we apply the appropriate corrections for unresolved and residual sources. In the following we will show some figures for results for spectra obtained with the combined V+W map. The results in the VV, WW and VxW cross spectra are similar and consistent. In figure 4 we show as an example (1) the power spectrum obtained when removing the 665 detected point sources and masking only the galaxy ( $C_\ell^{R,VW}$ ) and (2) the power spectrum obtained when masking (not removing) and using only the WMAP team’s KQ85 galactic and point source mask. We also show the difference between these spectra. These plots show well the agreement between masking and removing the detected sources when the appropriate corrections are used.

In figure 5 we show the difference between the spectra obtained with the biggest of our point source masks (galaxy and 2102 point sources with KQ85) and the smallest point source mask (galaxy plus 665 point sources detected in QVW) in case of only masking. This figure shows that the masking schemes and correction for unresolved point sources (i.e estimation of  $A_{PS}$ ) are well in agreement and that the weakest sources are well corrected for using the correction for unresolved sources instead of masking.

Eventually in figure 6 we show (1) the spectrum from the maps where we remove the 665 point sources detected in QVW ( $C_\ell^{R,VW}$ ) and masking only the galaxy and (2) the spectrum where we additionally mask the remaining of the total of 2102 point sources detected in all bands and templates  $C_{\ell,2102KQ85}^{R,VW}$ . In both spectra we have subtracted the best fit theoretical WMAP 7 spectrum. We see that both spectra are consistent with the theoretical model and with each other. One may expect that masking less has the advantage of more information and hence less fluctuations, this figure shows that this indeed the case (the black  $C_\ell^{R,VW}$  have clearly smaller fluctuations).

We also would like to stress that when only removing the detected point sources and not using any additional masking (a part of the galaxy) we are able to obtain consistent results

(see for instance, figures 4). Hence making it possible to estimate the power spectrum  $C_\ell$  without any point source masking!

#### 4. Skewness

If there were no point sources (resolved or unresolved) or other foregrounds in the sky maps, one would expect the skewness to be zero (with the exception of tiny deviations expected from a non-zero value of the  $f_{NL}$  parameter). The presence of point sources, though, introduces a positive skewness in the maps, since they give a positive contribution to the map, which does not have a negative counterpart. In order to test our approach of removing point sources we therefore are interested in how much (if at all) the skewness changes after point source removal, we do this for 10000 simulations in both V and W channels.

In analogy to Vielva et al. (2004) we define the skewness  $S_j$  at frequency  $j$  as:

$$S_j = \frac{1}{N_{out} \cdot \sigma_j^3} \sum_k \beta_{kj}^3, \quad (2)$$

where:

- $\beta_{kj}$  is the needlet coefficient at frequency  $j$  and pixel  $k$ , multiplied by the galactic mask;
- $N_{out}$  is the number of pixels outside the mask;
- $\sigma_j$  is the standard deviation of the needlet coefficients, defined as:

$$\sigma_j = \sqrt{\frac{1}{N_{out}} \sum_k \beta_{kj}^2}.$$

The first step in our skewness analysis is to get the error (in terms of the standard deviation) of the estimated skewness  $S_j$ . We do this by computing the skewness for 10000 simulated maps (in both the V and W channel) with CMB and noise, but no point sources, obtaining  $\sigma^{NoPS}$ . We also check how much and at which frequency  $j$  of the needlet skewness is introduced (in average) when there are point sources present. We therefore compute the average skewness  $\langle S_j^A \rangle$  of 10000 maps with noise, CMB and point sources.

The next step is to see what the skewness becomes when there are only unresolved sources. We simulate 10000 maps per channel with only unresolved sources, CMB and noise but no sources above the detection limit. We then calculate the average skewness  $\langle S_j^{onlyU} \rangle$

of these 10000 maps. The last step is to check whether the removal of point sources changes the skewness. In order to do this, we compute the average skewness  $\langle S_j^R \rangle$  for 10000 maps with the noise, CMB, unresolved point sources and the detected point sources removed using best fit models.

In figures 7 we show the average skewnesses  $\langle S_j^A \rangle$  (black line, stars),  $\langle S_j^{onlyU} \rangle$  (black line, squares) and  $\langle S_j^R \rangle$  (black line, plus-signs) for the two needlets we use in the simulations, namely for V standard needlets with  $B = 2$  and for W mexican needlets with  $p = 1$  and  $B = 1.8$ . These are the needlets which were used in Scodeller et al. (2012) and which were shown to be optimal for point source detection for these frequency channels. We also show the  $1\sigma^{NoPS}$  (continuous grey line) and  $2\sigma^{NoPS}$  (dashed grey line) intervals obtained from the standard deviation of simulated maps with no point sources. Eventually we also show an example of WMAP-data skewness (to be precise the absolute value of it, in order to see also the values for those frequencies which have slightly negative skewness) obtained in case of removing the detected point sources and masking the not removed ones from the 1116 detected point sources in channels directly or at  $5\sigma$  in templates and  $3\sigma$  in channels and from the wmap KQ85 mask (grey triangles).

As one would expect the skewness introduced by point sources (cf.  $\langle S_j^A \rangle$ ) is only  $\geq 1\sigma$  for needlet coefficients  $\beta_j$  with frequencies corresponding to small angular resolution. For instance, for the standard needlets (see top figure of plots 7) there is a skewness  $\geq 2\sigma$  only for frequencies  $j \in [8, 9]$ , which correspond to  $\ell$ -ranges<sup>3</sup>  $[128, 512]$  and  $[256, 1024]$ , which in turn indicatively corresponds to angular extensions of  $[1.4, 0.35]$  and  $[0.7, 0.17]$  degrees. This shows why there is no visible skewness at frequencies  $j$  smaller than 8, since it would imply that the point source is visible over an angular extension bigger than approximately 1 degree.

With respect to the skewness of maps where the detected point sources are removed ( $\langle S_j^R \rangle$ ), there is no substantial difference to the maps where there are only unresolved sources ( $\langle S_j^U \rangle$ ). This means that removing sources does not introduce skewness to the maps. If there were to be introduced a skewness from the removal of detected point sources it would mean that our estimate of the amplitude of the point sources is biased. This skewness plots hence consolidates hence the removing point sources approach.

---

<sup>3</sup>for standard needlets the  $\ell$ -range seen by a needlet at frequency  $j$  is given by  $[B^{j-1}, B^{j+1}]$ .

## 5. Conclusion

In this work we have studied (1) whether masking all the additional WMAP point sources reported in Scodeller et al. (2012) changes the WMAP estimate of the power spectrum compared to the spectrum obtained using the WMAP point source mask with much less point sources masked and (2) whether removing best fit source models instead of masking the detected point sources yields consistent results.

We compared the masking and removing approaches by making realistic simulations of 9000 maps with CMB, noise and point sources in each of the V and W channels (see section 2). In figures 1 (removed point sources) and 2 (difference between masked and removed point sources) we show that when estimating the  $C_\ell$  both approaches give consistent results. When computing the standard deviations (see figure 3) we see that, as expected since there is more information, the standard deviation of the power spectra when removing the point sources is smaller than when they are masked. We remark though that when removing point sources one has to account for the bias introduced by the error on estimating the point source position and amplitude, while when masking this errors introduce only a negligible bias.

When considering WMAP 7 year data (section 3) we also compare the two approaches estimating the CMB power spectrum. But additionally we also use different masks removing different fractions of the 2102 point sources detected in Scodeller et al. (2012). After removing respectively masking with the different masks (and correcting for the bias introduced by residual sources in case of removing), the two approaches and different masks give rise to different values of the amplitude  $A_{ps}$  of the unresolved point source contribution, the values are summarized in table 1. We remark that when using the mask of all 2102 point sources detected at  $5\sigma$  in either channels or templates, our estimate of  $A_{ps}$  is substantially smaller than the estimate from the WMAP-team:  $6.90 \pm 1.22$  (removing and masking) and  $6.60 \pm 1.29$  (only masking) versus  $9.0 \pm 0.7$  from the WMAP-team with the KQ85 mask (all amplitudes  $A_{ps}$  in units of  $[10^3 \mu K^2]$ ). Hence this new mask presents a big improvement.

We found that the power spectrum obtained when removing the 665 detected sources and using only the galactic mask (no point source mask), is fully consistent with the power spectrum obtained when masking all the 2102 detected sources. This shows (1) that it suffices to take into account only the sources detected by the WMAP team and correct for the remaining sources through the unresolved source correction and (2) that removing the best fit source models works as well as masking them. The advantage of removing is that for some CMB analysis methods (especially wavelet/filter based methods), the point source holes reduce significantly the sky fraction which can be used on the filtered maps. Note however, that in the case of point source removal, the appropriate correction for residual sources has to be applied. The removing approach is also verified with respect to skewness,

where we showed that the fact of removing point sources does not introduce any form of skewness, showing that the removal of point sources is an unbiased approach.

The different masks, the different pure point source maps for each DA (which can be used to remove sources in temperature maps to obtain clean maps) and the residual power corrections are available on: [http://folk.uio.no/frodekh/PS\\_catalogue/](http://folk.uio.no/frodekh/PS_catalogue/)

## 6. Acknowledgements

SSc would like to thank S.K. Næss for useful discussions. FKH acknowledges an OYI grant from the Norwegian Research Council. Super computers from NOTUR (The Norwegian metacenter for computational science) have been used in this work. We acknowledge the use of the HEALPix software package Górski et al. (2005) and the Legacy Archive for Microwave Background Data Analysis (LAMBDA) to retrieve the WMAP data set. This research has made use of data obtained from the High Energy Astrophysics Science Archive Research Center (HEASARC), provided by NASA’s Goddard Space Flight Center and of the NASA/IPAC Extragalactic Database (NED) which is operated by the Jet Propulsion Laboratory, California Institute of Technology, under contract with the National Aeronautics and Space Administration.

## REFERENCES

- Bajkova A. T., 2005, *Astron. Rep.*, 49, 947
- Bennett, C. L. et al., 2003, *ApJ*, 583,1
- De Zotti, G., Toffolatti, L., Argüeso, F., Davies, R. D., Mazzotta, P., Partridge R. B., Smoot, G.F. & Vitorio, N., *AIPConf.Proc.*476:204-223,1999
- De Zotti, G., Ricci, R., Mesa, D., Silva, L., Mazzotta, P., Toffolatti, L. & González-Nuevo, J., 2005, *A& A*, 431,893
- Gold, B., Odegard, N., Weiland, J. L., et al., 2011, *ApJS*, 192, 15
- Górski, K. M., Hivon, E., Banday, A. J., Wandelt, B. D., Hansen, F. K., Reinecke, M. & Bartelman, M., 2005, *ApJ*, 622, 759
- Hansen, F.K. ,Banday, A.J., Eriksen, H.K., Gorski,K.M & Lilje, P.B., 2006, *APJ*, 648, 784
- Herranz, D., Sanz, J. L., López-Caniego, M., González-Nuevo, J., 2006, *Proc. IEEE Symp., Signal Processing and Information Technology*, IEEE, New York, p. 541
- Hinshaw, G. et al., 2003, *ApJS*, 148, 135
- Hivon, E., Górski, K. M., Nettereld, C. B., Crill, B. P., Prunet, S., & Hansen, F. 2002, *ApJ*, 567, 2
- Hobson, M. P., Barreiro, R. B., Toffolatti, L., Lasenby, A. N., Sanz, J. L., Jones, A.W. & Bouchet, F. R., 1999, *MNRAS*, 306, 232
- Lanz, L. F., Herranz, D., López-Caniego, M., González-Nuevo, J., de Zotti, G., Massardi, M. & Sanz, J. L., *arXiv:1110.6877v1*
- Larson, D. et al., 2011, *ApJS*, 192, 16
- Marinucci, D., Pietrobon, D., Balbi, A., Baldi, P., Cabella, P., Kerkycharian, G., Natoli, P., Picard, D. & Vittorio, N., 2008, *MNRAS*, 383, 539
- Massardi, M., López-Caniego, M., González-Nuevo, J., Herranz, D., de Zotti, G. & Sanz, J. L., 2009, *MNRAS*, 392, 733
- Nolta, M. et al., 2009, *ApJS*, 180, 296-305
- Scodeller, S., Rudjord, O., Hansen, F.K., Marinucci, D., Geller, D & Mayeli, A., 2011, *ApJ*, 733, 121



Scodeller, S., Hansen, F.K. & Marinucci, D., 2012, ApJ, 753, 27

Tegmark, M. & de Oliveira-Costa, A., 1998, ApJL, 500, L83

Toffolatti, L., Argüeso Gómez, F., De Zotti, G., Mazzei, P., Franceschini A., Danese, L. & Burigana, C., 1998, MNRAS 297, 117

Vielva, P., Martínez-González, E., Barreiro, R.B., Sanz, J.L. & Cayón, L., 2004, ApJ, 609, 22

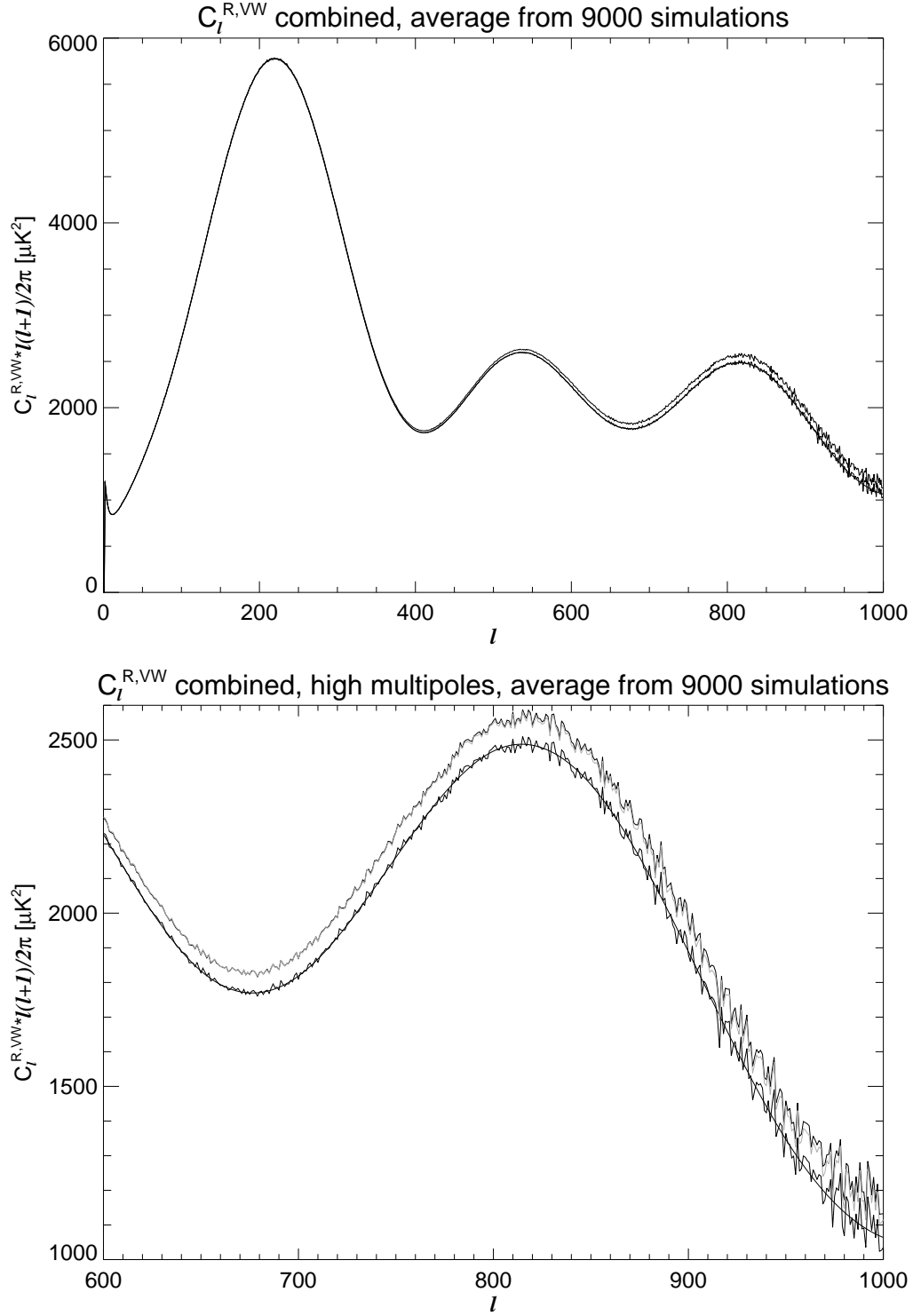


Fig. 1.— Average over 9000 simulations of the estimated power spectra when removing detected point sources for the combined map  $M_{VW}$ . Top: whole  $\ell$ -range, before and after correcting for the contribution of unresolved sources and over-plotted the input spectrum. Bottom: Zoom to higher multipoles  $\ell$ , the top black curve is before correcting for the bias introduced by point source residuals, the grey curve is the power after this correction, the bottom curve is after correcting for the unresolved source contribution and the smooth curve is the input power spectrum.

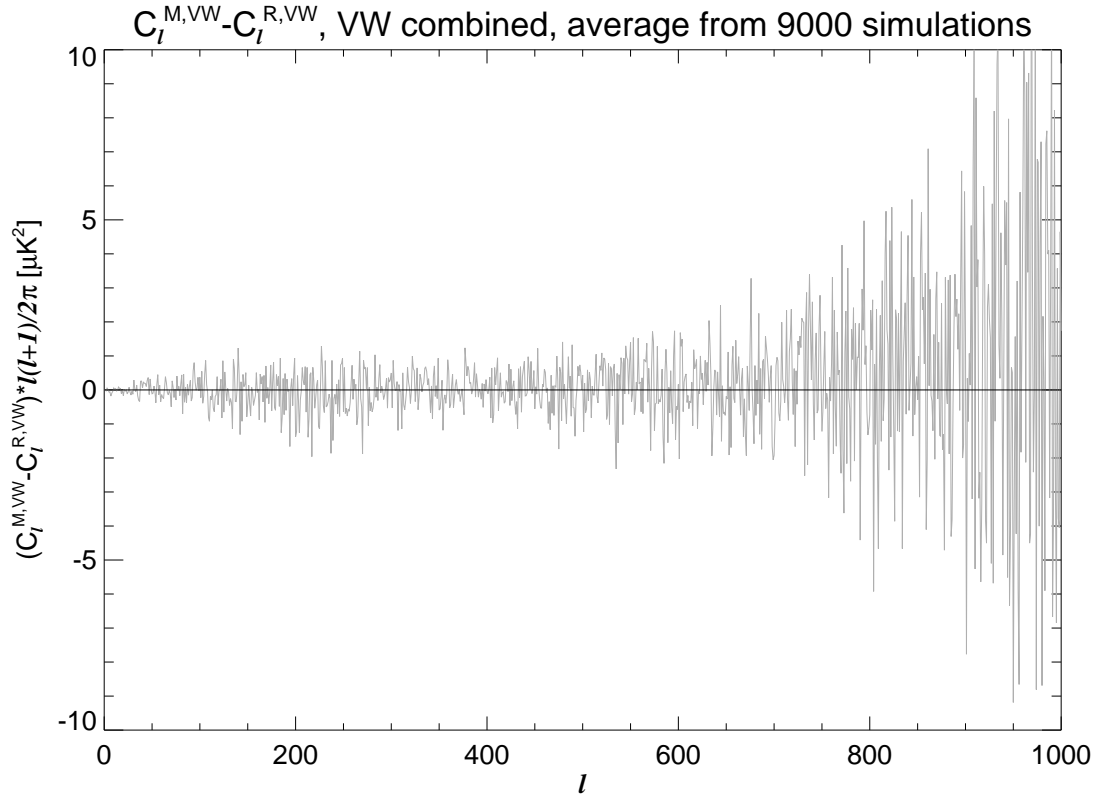


Fig. 2.— Difference between masked and removed average spectra from figure 1. The black line represents zero.

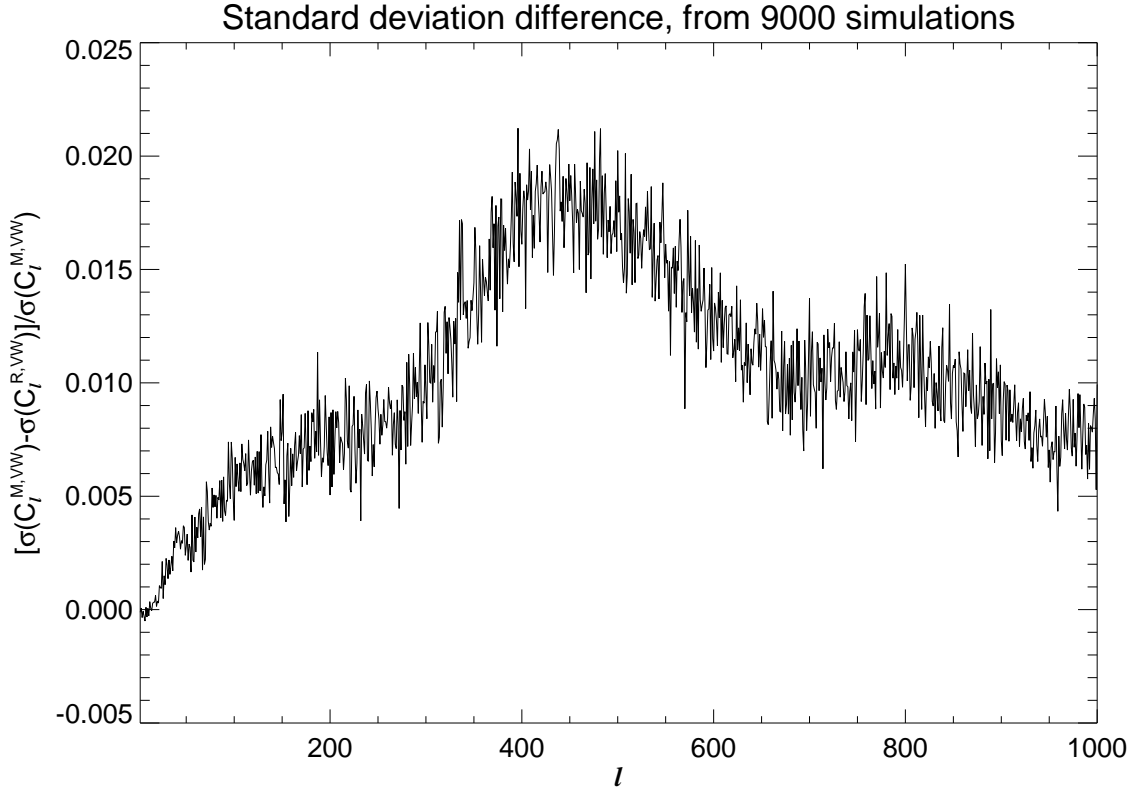


Fig. 3.— Relative difference of the standard deviation of the estimated power spectra of the combined map  $M_{VW}$  when masking or removing, normalised to the standard deviation of the standard approach (i.e. masking). Based on 9000 simulations.

Table 1: Amplitude of the unresolved point source contribution  $A_{ps}$  normalised to 40.7 GHz in  $10^3 \mu K^2$ . The different mask names are defined in section 3.1

	Value	Error	sky-frac <sup>a</sup>		Value	Error	sky-frac <sup>a</sup>
				$A_{ps}^{M,KQ85}$	9.18	1.14	78.3%
$A_{ps}^R$	10.82	1.06	80.6%	$A_{ps}^M$	10.17	1.12	78.9%
$A_{ps,ext}^R$	9.64	1.07	80.4%	$A_{ps,ext}^M$	9.48	1.13	78.7%
$A_{ps,extKQ85}^R$	8.22	1.10	79.4%	$A_{ps,extKQ85}^M$	8.04	1.16	77.6%
$A_{ps,1116}^R$	9.38	1.10	79.4%	$A_{ps,1116}^M$	8.69	1.17	77.6%
$A_{ps,1116KQ85}^R$	7.53	1.13	78.5%	$A_{ps,1116KQ85}^M$	7.34	1.19	76.8%
$A_{ps,2102}^R$	8.51	1.20	76.8%	$A_{ps,2102}^M$	7.75	1.27	75.0%
$A_{ps,2102KQ85}^R$	6.90	1.22	76.0%	$A_{ps,2102KQ85}^M$	6.60	1.29	74.3%

---

Note. — Unlike for the simulations, the error on  $A_{ps}$  is obtained by the expression in Hinshaw et al. (2003).

<sup>a</sup>The kept sky fraction of the mask.

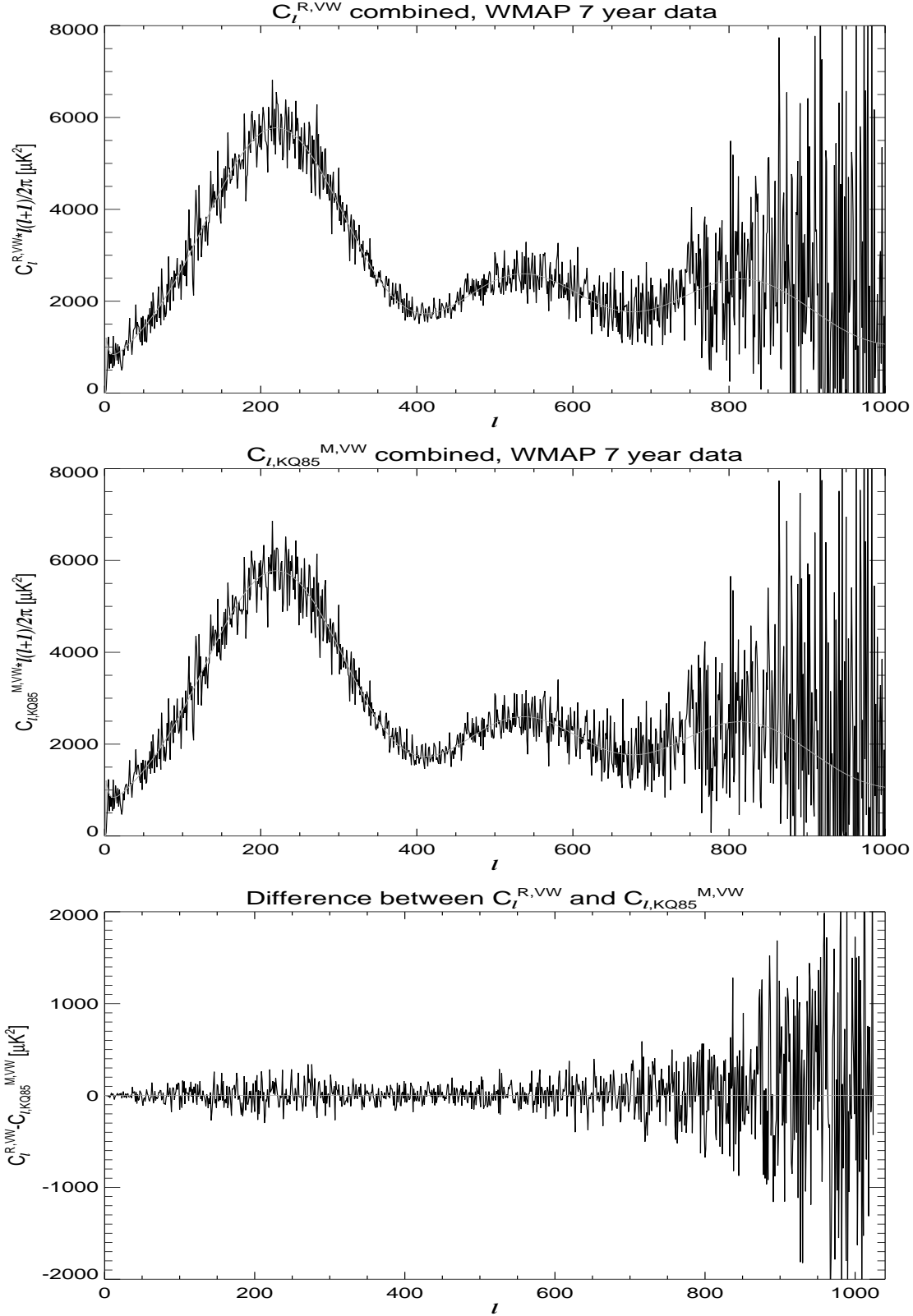


Fig. 4.— Examples of spectra obtained from the combined map  $M_{VW}$  for WMAP 7 year data. Top: when removing the 665 detected sources and masking the galaxy. Middle: when using the WMAP KQ85 galactic and point source mask (not removing). The grey line is the the best fit WMAP-spectrum. Bottom: difference between the spectra grey line being zero.

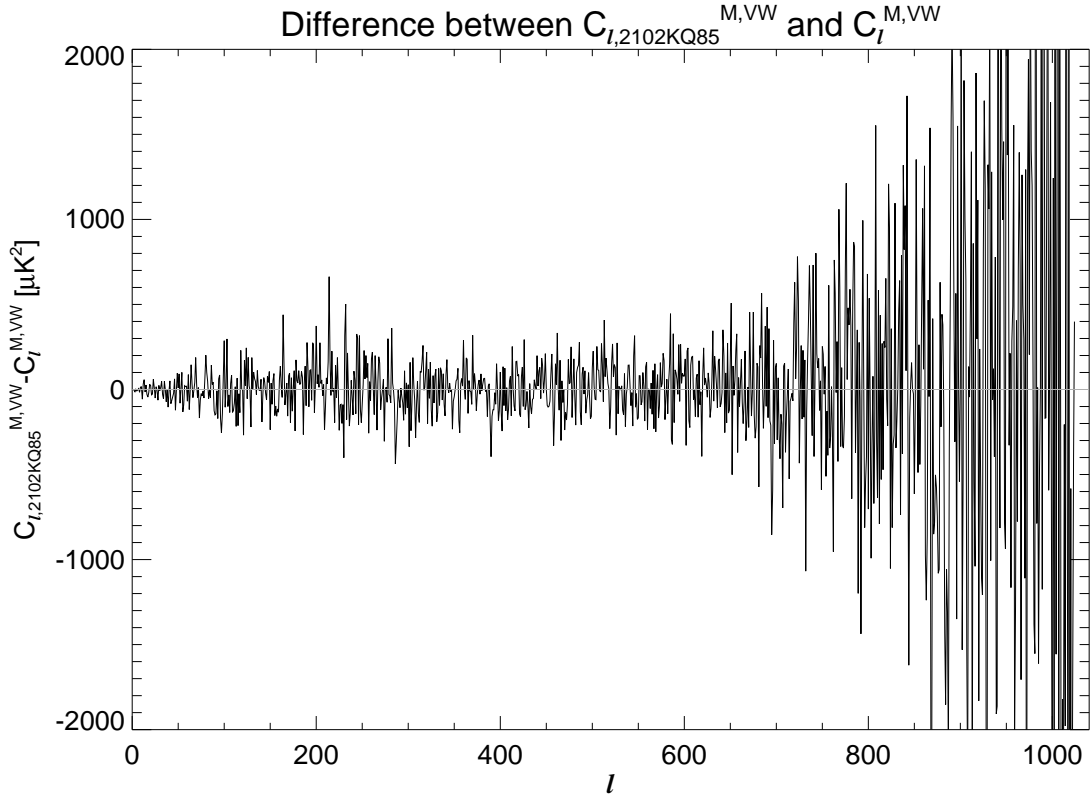


Fig. 5.— Difference between the spectrum obtained from the combined maps of WMAP 7 year data with the biggest point source mask and the one obtained with the smallest point source mask. The grey line represents zero.

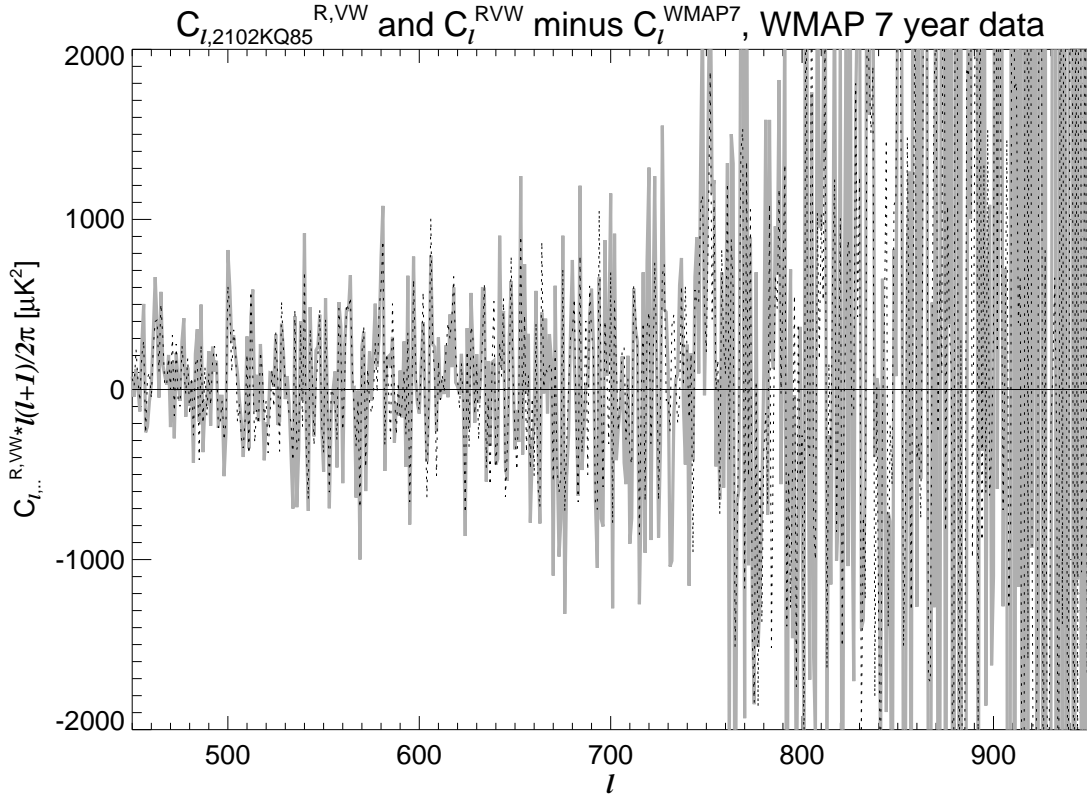


Fig. 6.— High multipole range of the spectra  $C_{\ell,2102KQ85}^{R,VW}$  (grey, continuous) and  $C_{\ell}^{R,VW}$  (black, dotted) of the combined map  $M_{VW}$ . The best fit theoretical WMAP 7 spectrum has been subtracted in both cases. The smooth black line represents zero.



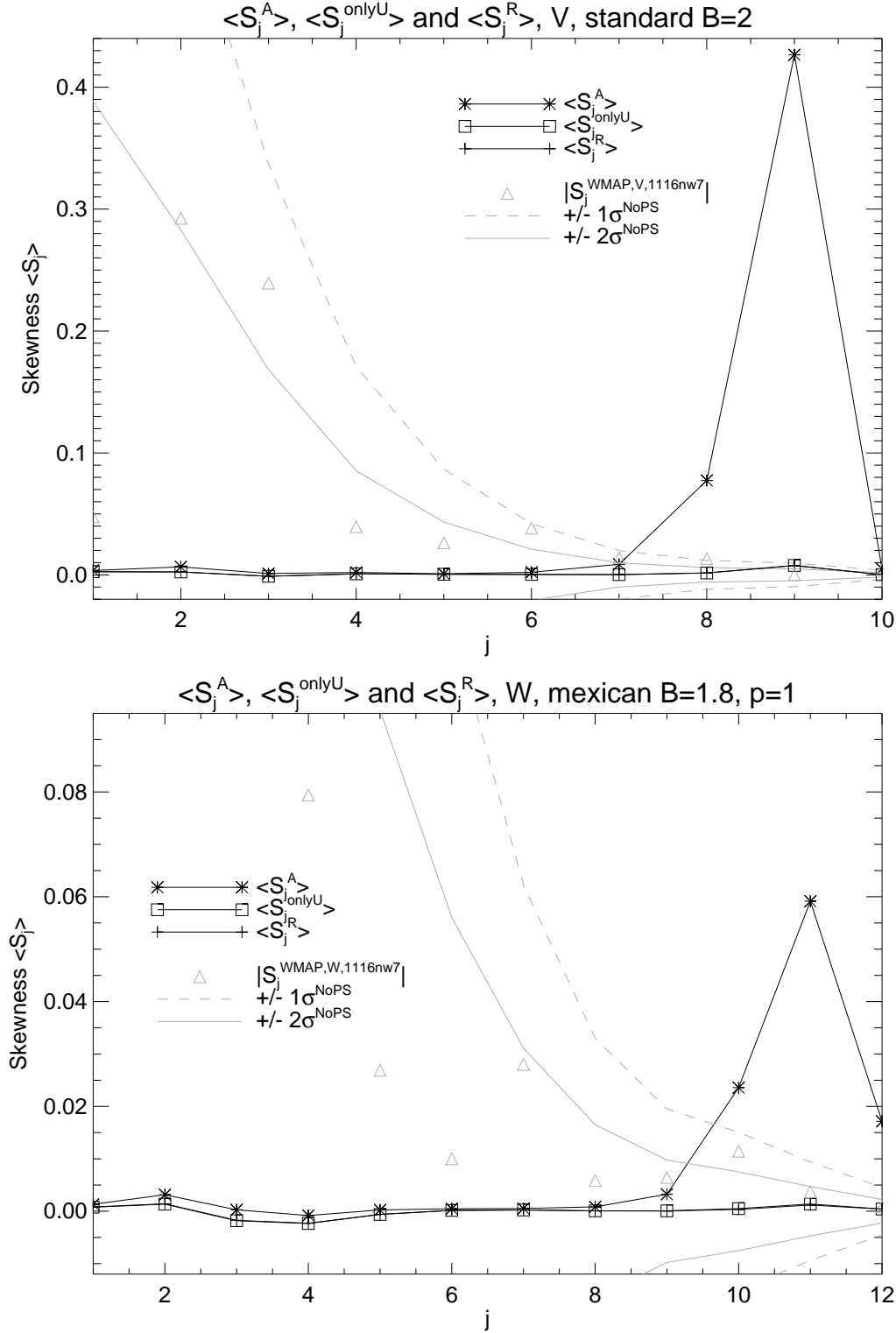


Fig. 7.— Average skewnesses  $\langle S_j^A \rangle$  (black line, stars),  $\langle S_j^{\text{onlyU}} \rangle$  (black line, squares) and  $\langle S_j^R \rangle$  (black line, plus-signs). The continuous grey lines represent  $\pm 1\sigma$ , the dashed grey lines  $\pm 2\sigma$ . The grey triangles show the absolute value of the skewness with WMAP data (see text). Top: for the simulated maps of the V channel, with standard needlets and  $B = 2$ . Bottom: for the simulated W channel maps, with mexican needlets with  $B = 1.8$  and  $p = 1$ .